

Article

Experimental Analysis and Process Modeling of Carbon Dioxide Removal Using Tuff

Emanuele Bonamente ^{1,2,*}, Andrea Aquino ², Andrea Nicolini ^{1,2} and Franco Cotana ^{1,2}

¹ Department of Engineering, University of Perugia, Via G. Duranti, 06125 Perugia, Italy; andrea.nicolini@unipg.it (A.N.); cotana@crbnet.it (F.C.)

² Interuniversity Research Center on Pollution and Environment, University of Perugia, Via G. Duranti 67, 06125 Perugia, Italy; aquino@crbnet.it

* Correspondence: emanuele.bonamente@unipg.it; Tel.: +39-075-585-3914

Academic Editors: Francesco Asdrubali and Pietro Buzzini

Received: 30 September 2016; Accepted: 26 November 2016; Published: 2 December 2016

Abstract: Removal of carbon dioxide via selective adsorption is a key process to obtain consumer-grade natural gas from biogas and, more generally, CO₂ capture and sequestration from gaseous mixtures. The aim of this work is the characterization and classification of a natural alternative to synthetic zeolites that could be used as a carbon dioxide adsorbent. Tuff particulate, easily available as a byproduct of the construction industry, was tested with different laboratory procedures to verify its suitability for CO₂ removal applications. Relevant physical and adsorption properties were measured during an intensive experimental campaign. Porosity, pore size distribution, and specific surface area were obtained with mercury intrusion porosimetry. Adsorption isotherms and saturation curves were obtained using two custom experimental apparatuses. The selective adsorption was finally modeled using an original phenomenological parameterization, and a simplified simulation of the process was performed using a computational fluid dynamic approach, validated against observed data. Results show that natural zeolites represent a very promising and sustainable alternative to synthetic zeolites in pressure swing adsorption processes for CO₂ removal.

Keywords: carbon dioxide (CO₂) removal; biogas upgrading; natural zeolites; computational fluid dynamic (CFD) simulations; adsorption

1. Introduction

The worldwide economic and population growth continue to be the most important drivers of increases in carbon dioxide (CO₂) emissions, fossil fuel combustion, and industrial processes contributing to approximately 78% to the total emission increase [1]. Effective solutions for reducing the concentration of CO₂ in the atmosphere are: energy-efficiency enhancement, including building design [2] and urban planning [3,4], reduction of CO₂ emissions exploiting renewable energy resources [5], and carbon capture and sequestration [6,7]. The CO₂ removal with adsorption-based techniques can be easily pursued for several applications thanks to their low operational requirements, ease of control, and high efficiency [8].

Selective physical adsorption of gas mixture species can be obtained with pressure swing adsorption (PSA) coupled with vacuum swing adsorption (VSA) [9,10]. Common applications are the removal of carbon dioxide from CO₂/CH₄ mixtures to produce purified natural gas and biomethane [11–13] and carbon capture and sequestration [14].

The use of an appropriate adsorbent is necessary to successfully design an adsorption-based apparatus. Desirable characteristics of an optimal adsorbent are a high adsorption capacity, a low regeneration heat, and a low purchase cost [15]. Several adsorbents have been proposed for carbon

dioxide adsorption, including activated carbon [16], T-type zeolite [17], 13X and 5A zeolites [18], metal organic frameworks [19], and clays [20].

Tuff is a highly-porous volcanic rock commonly utilized by vernacular architecture, and particularly widespread in Italy as it is abundant at the surface and easy to manufacture [21,22]. It is a mix of natural zeolites and its composition makes it a very interesting alternative to synthetic zeolites for CO₂ adsorption via PSA techniques. It is also available in small particles, at almost no cost except for shipping, as a byproduct of the building industry. The aim of this work is to quantitatively characterize the adsorption capacity of tuff and provide the basic information for its exploitation in PSA applications. Several experimental activities were performed: mercury intrusion porosimetry [23] was used to determine the tuff superficial pore size, pore distribution, and other relevant physical properties. A custom apparatus was set up in order to reproduce the adsorption process under controlled working conditions and measure the saturation level of tuff and the amount of adsorbable CO₂ before the breakthrough point is reached. Data obtained from the experimental campaign were used to model the CO₂ adsorption using a computational fluid dynamic (CFD) approach, with the goal of developing a useful tool for real PSA applications design. A second custom apparatus was designed to measure the maximum adsorption capacity of natural and synthetic zeolites under equilibrium conditions via a volumetric method [24,25]. A range of equilibrium pressures at different operative temperatures was investigated and a comparison between the adsorption performance of tuff and synthetic zeolite 13X is presented.

Section 2 introduces the used material, pretreatment techniques, and the laboratory characterization of particle properties. A detailed description of the custom experimental apparatus is given in Section 3, and results for data analysis and modeling are presented along with the used methodology. Section 4 contains a discussion of the results. Conclusions are summarized in Section 5.

2. Tuff Physical Properties

2.1. Tuff Samples

In this work, tuff samples provided by the “*Piandirena*” quarry located in Sorano (GR), Italy, were used. The chemical composition, according to a previous analysis [26], includes chabazite (65 ± 5)%, phillipsite (3 ± 2)%, K-feldspate (10 ± 3)%, augite (2 ± 1)%, mica (5 ± 2)%, and volcanic glass (15 ± 4)%.

For comparison purposes, three different samples were initially separated from the same stock. Before each experimental activity, samples were pre-treated and weighted. Pre-treatment is a crucial part of the process, and it was found that the optimal procedure consists in removing tuff dust off of the tuff particles surface using compressed air or running water and a subsequent thermal regeneration. The regeneration and activation step is needed to ensure an optimal performance of zeolites, paying attention to avoid irreversible changes in their structure [27]. No differences, in terms of CO₂ adsorption capacity, were observed between air and water cleaning. Thermal regeneration, on the other hand, was found to be a relevant parameter.

As described in the following sections, two different thermal regeneration temperatures were considered: 220 °C and 350 °C. In both cases regeneration took place overnight for a period of approximately 12 h. The first regeneration temperature was used to reproduce the same conditions of previous literature works [27]. Thermogravimetric analysis of exhausted tuff particles, however, shows a measurable mass loss up to approximately 350 °C. This second regeneration temperature was also considered during the adsorption isotherm experiments to test the maximum adsorption capacity of the material.

During adsorption experiments, carbon dioxide and nitrogen, with a purity of 99.7% and 99.999%, respectively, were used. Here we have made the assumption that nitrogen is negligibly adsorbed by tuff particles. This assumption is supported from preliminary results showing no detectable adsorption using an experimental layout similar to that in Section 3.1. During the experimental campaign, nitrogen

was used either as purge gas or in place of methane to reproduce the required inlet gas mixture. Future analyses will be conducted in a safe environment using a real CH₄/CO₂ mixture.

2.2. Mercury Intrusion Porosimetry

The performance of a porous solid used as an adsorbent is highly influenced by its internal pore structure [26,28,29] and, hence, it is necessary to have a detailed knowledge of the geometry and topology of the internal pore network. To this aim, several techniques are available [30–33]. Mercury intrusion porosimetry was used in this work to determine the pore spatial distribution of tuff and other properties, such as porosity and bulk (i.e., particle) density. With this technique, however, it is only possible to explore pore sizes down to mesopore scales: a complete characterization of pore distribution should explore smaller sizes, down to the micropore scale, which are more relevant for adsorption processes of natural zeolites, and it would require different experimental techniques.

Tuff samples were analyzed in sequence using two porosimeters (mod. Pascal 140 and mod. Pascal 240 Thermoscientific™, Waltham, MA, USA), each one characterized by two different maximum working pressures. The low-pressure porosimeter can operate to a maximum pressure of 400 kPa, measuring pores with diameters between 4 μm and 120 μm. The high-pressure porosimeter can operate to a maximum pressure of 200 MPa, measuring pores with diameters between 0.0074 μm and 15 μm.

Measured data (Table 1) show a wide range of variability. This is most likely related to the high heterogeneity of physical and chemical properties of tuff [26], and to the low capacity of porosimeters, which can characterize only small samples (few grams, i.e., a few particles) at a time. The measured pore size distribution is shown in Figure 1. According to results, the tuff surface is mainly characterized by macropores with a diameter between 2 μm and 4 μm, with a specific volume of $1.31 \times 10^{-4} \text{ m}^3/\text{kg}$.

The skeletal density $\rho_{skeleton}$ (i.e., density of tuff solid matter only) was calculated using the following equation:

$$\rho_{skeleton} = \frac{\rho_{particle}}{(1 - P)} \quad (1)$$

where $\rho_{particle}$ and P are the measured particle density and porosity, respectively.

Table 1. Tuff physical properties.

Total Porosity (%)	Skeletal Density (kg/m ³)	Particle Density (kg/m ³)	Average Pore Diameter (μm)	Particle Size (Diameter) (mm)
20.1% to 36.3%	1522 to 1535	977 to 1215	1.42 to 4.64	3 to 10

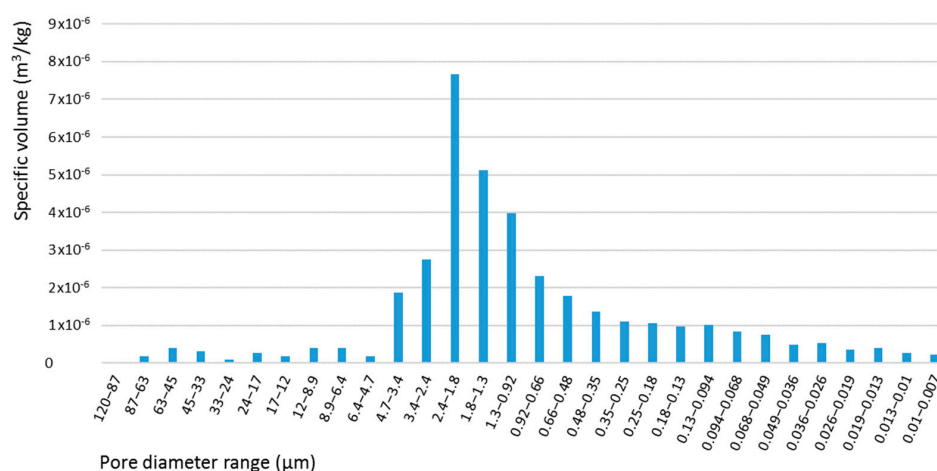


Figure 1. Macro- and mesopore size distribution for tuff particles.

3. Adsorption Analyses

The characterization of the adsorption properties of tuff was performed following two different approaches and running independent experiments. The selective adsorption of CO₂ from a gaseous mixture in the transient regime was investigated monitoring the inlet and outlet composition flowing through a cartridge containing tuff (Section 3.1). The maximum adsorption capacity at equilibrium was evaluated using a temperature- and pressure-controlled apparatus (Section 3.2). CFD simulations of the adsorption process in transient regime is also presented in the subsection of Section 3.1.

A preliminary analysis of N₂ adsorption in tuff particles was carried out under ambient conditions using a simplified layout similar to that in Figure 2. A sample of 533.09 g was flown with pure N₂ until equilibrium is reached. The sample weight increase is 0.23 g, resulting in less than 0.0005 kg_{N₂}/kg_{Tuff}. The same procedure was also performed using pure CO₂: the mass increase is 40.36 g, corresponding to an approximate adsorption capacity of 0.076 kg_{CO₂}/kg_{Tuff}, which is consistent to that shown in more accurate results from adsorption isotherms (see Section 3.2).

3.1. Saturation Curves

When a mix of inert (e.g., N₂) and adsorbable (e.g., CO₂) gases is flown through an adsorbent (e.g., tuff), the outlet composition varies as the amount of adsorbed gas increases and the adsorbent becomes saturated, losing its ability of capturing further gas molecules. Common applications, like biogas upgrading, require the outlet mixture not to exceed some reference level of CO₂ (i.e., the breakthrough point). Transient-regime analyses of the adsorption process that monitor the gas composition at outlet as a function of the cumulative adsorbed CO₂ are often carried out using breakthrough (or saturation) curves [34]. In particular, they are necessary to characterize the saturation level for a defined quantity of adsorbent under a specific set of operative conditions. After each measurement, the adsorbent cartridge has to be refilled with freshly pre-treated adsorbent. The exhausted adsorbent can be regenerated for reuse. The regeneration temperature used during this analysis is 220 °C.

The laboratory setup used to measure tuff saturation curves is shown in Figure 2. It includes a gas mixer (mod. MM-Flex WITT-Gasetechnik™, Witten, Germany), a flow rate meter (mod. SK-25 Kimmon™, Tokyo, Japan), an adsorption column cartridge (a PVC cylinder of 60 mm diameter and 600 mm length), a vent, and an infrared gas analyzer (mod. ABE 1500 AB Energy™, Biella, Italy). Two open-cell polyurethane foam discs (approximately 30 mm length) were placed at the internal ends of the cartridge to contain the tuff particles. The resulting bed volume is approximately 1.5 L. Before the data acquisition was started, the column was purged with a pure nitrogen flow, until a null concentration of CO₂ was measured at the outlet. The experiment was performed flowing a synthetic gas mixture of CO₂ and N₂ through a cartridge loaded with tuff samples of approximately 0.6 kg. The outlet CO₂ concentration vs. time was measured for each sample until full saturation was reached (i.e., when the outlet CO₂ concentration equals the inlet CO₂ concentration). Data were recorded every 5 s.

Six saturation curves were measured using two sub-samples from each of three different tuff samples A, B, and C. Before each measurement, the samples were pretreated according to the procedure reported in Section 3.1. Figure 3 shows the CO₂ concentration, measured at the cartridge outlet, as a function of time. The different performance of samples are mainly due to different operating conditions (i.e., inlet CO₂ concentration, inlet flow rate, sample weight), as reported in Table 2.

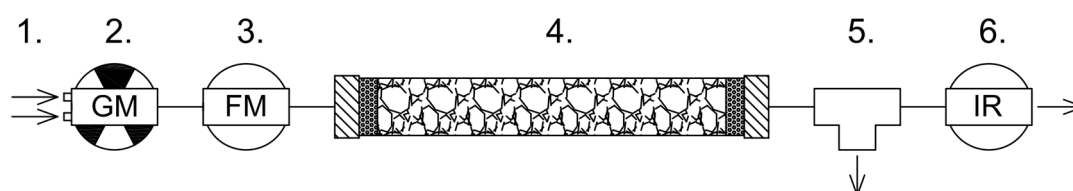


Figure 2. Layout of the saturation curve experimental apparatus: (1) gas feed inlet; (2) gas mixer; (3) flow meter; (4) cartridge; (5) vent; and (6) infrared gas analyzer.

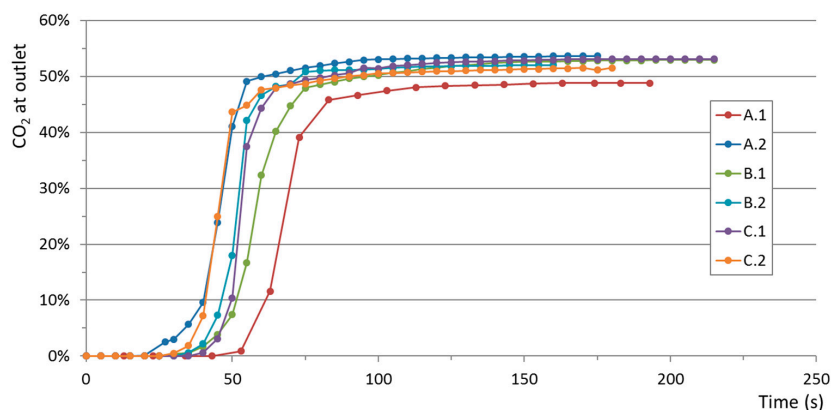


Figure 3. Outlet CO₂ concentration vs. time for the six sub-samples.

Table 2. Operative conditions of saturation analyses.

Sample	Inlet Flow Rate (Min–Max)		Sample Weight (g)	Inlet Mixture Composition (N ₂ %–CO ₂ %)	Analysis Duration (s)
	(L/s)	(kg/s)			
A.1	0.33–0.46	$(0.422–0.588) \times 10^{-3}$	615.04	51.2%–48.8%	193
A.2	0.24–0.50	$(0.322–0.671) \times 10^{-3}$	522.66	46.4%–53.6%	175
B.1	0.30–0.52	$(0.400–0.693) \times 10^{-3}$	594.94	47.1%–52.9%	215
B.2	0.32–0.50	$(0.423–0.660) \times 10^{-3}$	543.26	48.0%–52.0%	160
C.1	0.30–0.48	$(0.401–0.641) \times 10^{-3}$	591.40	46.9%–53.1%	215
C.2	0.32–0.48	$(0.421–0.631) \times 10^{-3}$	519.35	48.5%–51.5%	180

A more precise estimate of general tuff adsorption properties can be obtained with a deconvolution of observed quantities from the particular operative condition. Since the saturation level of tuff particles, and not time, directly regulates the adsorption process, another way of presenting saturation curves is proposed in Figure 4. Here the outlet CO₂ concentration is shown as a function of the cumulative amount of CO₂ flown through the cartridge per unit mass of tuff (kg_{CO₂}/kg_{Tuff}). The inlet flow rate was measured at each time step, and the resulting inlet amounts of CO₂ and N₂ are computed considering the known gas composition, which is constant during each experiment. It can be observed that the spread among all the samples is reduced with respect to the behavior shown in Figure 3.

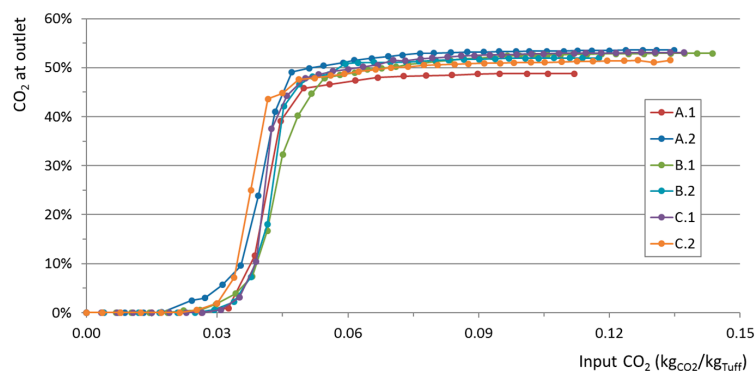


Figure 4. Outlet CO₂ concentration vs. input CO₂ for the six sub-samples.

The breakthrough point was estimated considering the biomethane quality requirements reported in national technical regulations [35], which recommend an outlet CO₂ concentration not exceeding 3% in volume. According to the results shown in Figure 4, the maximum amount of CO₂ that can flow through a tuff adsorption cartridge, before the breakthrough point is reached, is between 0.029

and $0.036 \text{ kg}_{\text{CO}_2}/\text{kg}_{\text{Tuff}}$. This result was obtained with an inlet gas pressure equal to the atmospheric pressure (the vent in Figure 2 does not allow the cartridge to pressurize, having a CO_2 partial pressure of approximately 0.05 MPa) and an outflow gas temperature in the range 18–19 °C.

Finally, Figure 5 shows the cumulative adsorbed CO_2 as a function of input CO_2 , per unit mass of tuff. Before the breakthrough point, all samples show the same behavior (all of the input CO_2 is effectively adsorbed and the slope of the curves is 1). Different samples deviate from linearity at different values of input CO_2 according to what shown in Figure 4.

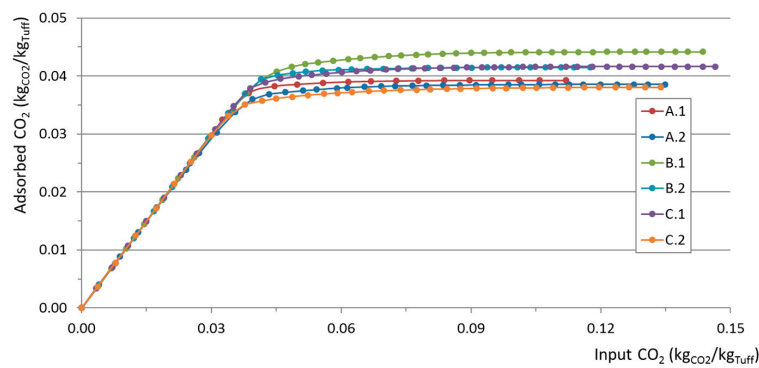


Figure 5. Adsorbed CO_2 vs. input CO_2 for the six sub-samples.

CFD Simulations

Computational fluid dynamics simulations were developed using Ansys Fluent 16.2 [36] in order to study the CO_2 adsorption with tuff in transient regime. The adsorption process was modeled considering a fluid mixture of chemical species (CO_2 and N_2), flowing through a cylindrical adsorption column packed with a porous material (tuff). As a first step, the geometrical domain was developed using the same dimensions of the saturation curve apparatus. The 3D model features a total bed volume of 0.0015 m^3 (approximately 0.06 m diameter and 0.54 m length). The total bed porosity, defined as the ratio between the total vacuum volume (inter- and intra-particle vacuum) and the total volume occupied by the bed, is 0.76–0.79. For all of the simulations, the energy equation, the standard k - ϵ turbulence model, and the mixed species transport model were used in order to consider the binary species mixture and transport processes in a turbulent regime. A non-reacting two-species mixture is considered, resulting in separate sets of mass, momentum, and energy conservation equations [37]. The mixture density is obtained using the compressible ideal gas model. The diffusivity of the mixture is computed with the multi-component law [38]. The porous media is assumed to be isotropic and the related pressure losses are quantified with the Ergun equation [38]. All of the cases are simulated in the transient regime with a 1 s time step (a first step after 0.1 s was also computed).

To simulate the CO_2 adsorption process, a source term (S_m), specific for each cell of the domain, is included in the mass balance equation:

$$\frac{\partial \rho}{\partial t} + \nabla \cdot (\rho \vec{v}) = S_m \quad (2)$$

User-defined functions were implemented to model the source term as a selective mass sink (only CO_2 is adsorbed) characterized by a decreasing adsorption rate as a function of the saturation level. The cell saturation level (x , Equation (3)) is defined as the ratio of the cumulative adsorbed CO_2 (q_{ads}) and the maximum adsorbable amount (q_{ads}^{max}). At the beginning of the process x equals 0 (fresh tuff), and it becomes 1 for fully-saturated cells (exhausted tuff). The cell adsorption rate (\dot{q}_{ads}) depends on the saturation level, and it is maximum for $x = 0$ and zero for $x = 1$. The adsorption rate as a function of the saturation level was modeled according to Equation (4). The saturation function Y (Equation (5)) represents a tentative and original parameterization that relates the adsorption rate to the saturation

level via a phenomenological parameter (a). The saturation parameter a used in the simulations was obtained from a fit to observed data as shown in Figure 6. The total adsorbed CO₂ of the model (blue) equals the observed value (green) and the behavior around the breakthrough point is well reproduced.

A model validation was performed based on the comparison between simulations and experimental data. The boundary conditions used for each run and the related simulation case are shown in Table 3. Constant average values were used for inlet flow rates. Examples of the validation results are shown in Figure 7. Examples of the simulation outputs are shown in Figure 8.

$$x = \frac{q_{ads}}{q_{ads}^{max}} \tag{3}$$

$$\dot{q}_{ads}(x) = \dot{q}_{ads}(0) \times Y(x) \tag{4}$$

$$Y(x) = \frac{\exp(x^a) - e}{1 - e} \tag{5}$$

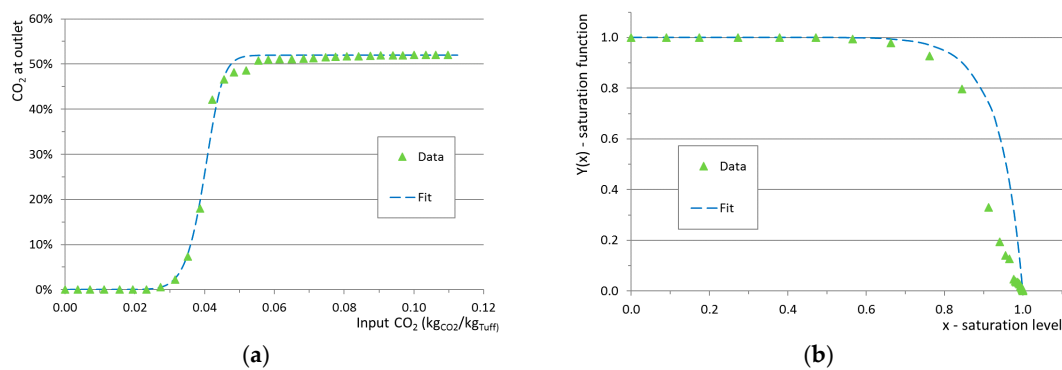


Figure 6. Fit for saturation parameter evaluation (B.2 sample). (a) outlet vs inlet CO₂; (b) saturation function vs saturation level.

Table 3. Boundary conditions for CFD simulations.

Validation Case	Sample Weight	Inlet Flow Rate	CO ₂ Volume Fraction	CO ₂ Mass Fraction	q_{ads}^{max}	a
	(kg)	(kg/s)	(-)	(-)	(kgCO ₂ /m ³)	(-)
A.2	0.5227	0.585×10^{-3}	0.536	0.645	16.87	7
B.1	0.5949	0.591×10^{-3}	0.529	0.638	23.16	7
B.2	0.5433	0.591×10^{-3}	0.520	0.630	19.01	11
C.1	0.5194	0.579×10^{-3}	0.515	0.655	17.08	8

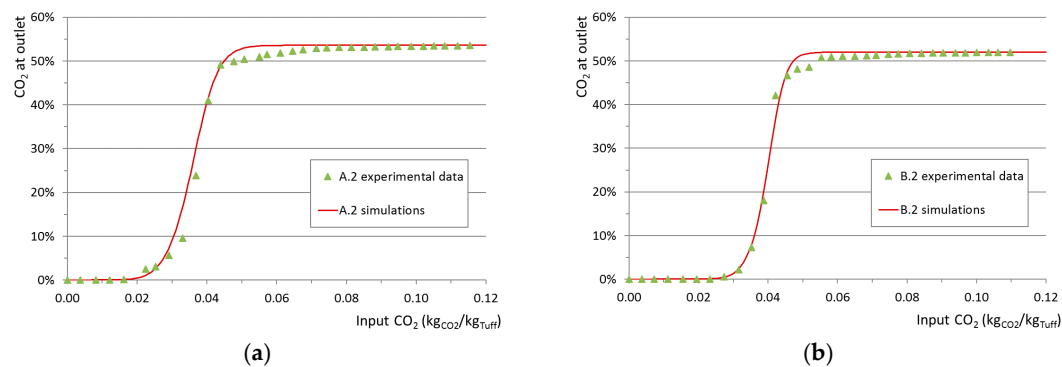


Figure 7. A.2 (a) and B.2 (b) CFD simulations (red) vs. experimental data (green).

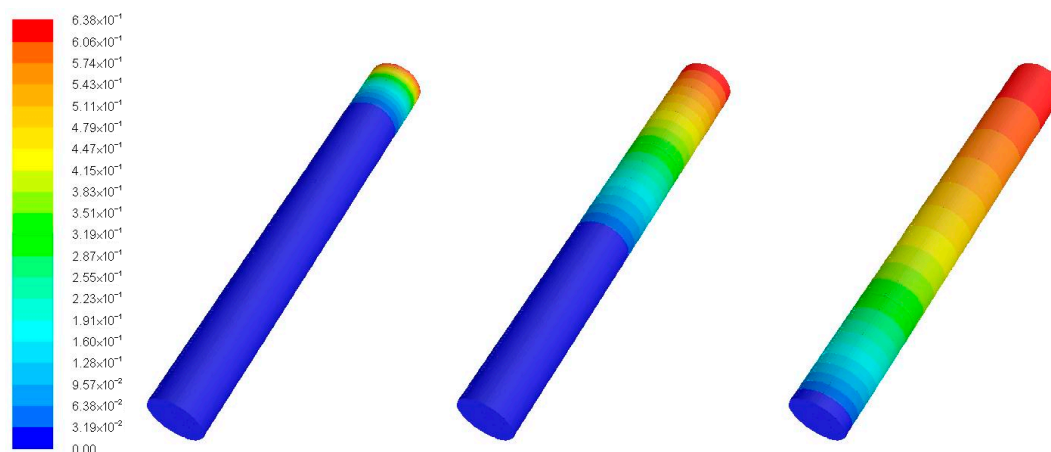


Figure 8. CO₂ mass fraction inside the cartridge after 0.1 s (left); 1 s (center); and 10 s (right) from CFD simulations.

3.2. Adsorption Isotherms

The adsorption equilibrium happens when, under specific (and fixed) boundary conditions, the adsorbent is fully saturated and it is no longer able to adsorb more. Adsorption equilibrium can be measured with different methods classified as volumetric, gravimetric, and chromatographic [25]. In the presented work, the volumetric method, successfully used in other similar works [24], was applied. This approach consists in letting a known amount of adsorbable gas expand inside a known volume containing the adsorbent. Measuring the equilibrium pressure it is possible to estimate the adsorbed amount. It was also found that reliable results can be obtained using the ideal gas approximation.

A custom experimental apparatus was setup with the aim of measuring adsorption isotherms, i.e., the maximum adsorbable CO₂ of tuff for a given temperature as a function of CO₂ equilibrium pressure. The apparatus is shown in Figure 9. It is an airtight system that consists of two known volumes (V_s and V_r) connected, with a switchable manifold, to gas feed line, a vacuum pump (mod. V-700 Büchi™) and a digital manometer (mod. LEO1 Keller™). The system is immersed in a thermostatic bath in order to maintain a constant set temperature (T_b).

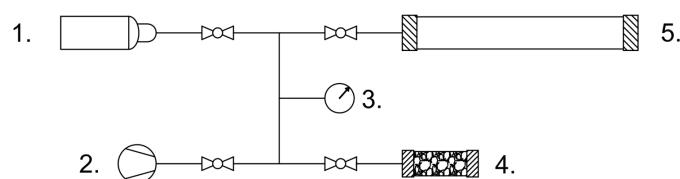


Figure 9. Layout of the adsorption isotherm experimental apparatus: (1) gas feed inlet; (2) vacuum pump; (3) manometer; (4) sample volume; and (5) expansion (reference) volume.

V_s hosts the tuff sample, V_r is a reference volume used to measure the amount of CO₂ in the system before the adsorption process. The measurement is a three-step procedure. As a first step, a known amount of tuff is placed inside V_s and the system is evacuated down to mid-vacuum conditions (approximately 15 mbar). During the second step, V_s is isolated and the V_r volume is filled with the desired amount of CO₂. In order to guarantee that no residual air remains inside V_r , the system is purged with CO₂ right after V_s is isolated. Once the system reaches the thermal equilibrium with the bath, the amount of CO₂ can be estimated measuring the pressure and using the ideal gas approximation (the total volume is given by V_r and the piping volume). In the final step, the CO₂ is allowed to expand inside V_s and the equilibrium pressure is measured after the adsorption process

ends. The amount of unadsorbed CO₂ is measured considering the final volume V_{eq} , which includes V_s , V_r , and the piping volume. As a result, the amount of adsorbed CO₂ as a function of the equilibrium pressure can be estimated as the difference between initial and unadsorbed CO₂. All system volumes are summarized in Table 4.

For each point of the saturation curve, pressures were measured only at thermal equilibrium. In the second step, the thermal equilibrium is reached typically after 1–2 min, and the pre-expansion pressure (P_0) is used to compute the initial amount of CO₂ (n_0) (Equation (6)). In the last step, after the CO₂ is adsorbed and the thermal equilibrium is reached (typically in 8–10 min), the equilibrium pressure (P_{eq}) is used to compute the unadsorbed CO₂ amount (n_f) (Equation (7)). Thanks to CO₂ purge, the only residual air inside the system is given by the vacuum pressure inside V_s , and it can be neglected after CO₂ expansion. The amount of adsorbed CO₂ (n_{ads}) is computed according to Equation (8).

$$n_0 = \frac{P_0 \times V_r}{R \times T_b} \quad (6)$$

$$n_f = \frac{P_{eq} \times V_{eq}}{R \times T_b} \quad (7)$$

$$n_{ads} = n_0 - n_f \quad (8)$$

Table 4. Samples weight at collecting time and pre-treatments.

Component	Description	Volume (m ³)
V_s	Sample volume	$(3.22 \pm 0.06) \times 10^{-5}$
V_r	Pre-expansion and pre-adsorption volume	$(9.721 \pm 0.003) \times 10^{-4}$
V_{eq}	System total volume and equilibrium volume	$(1.0008 \pm 0.0007) \times 10^{-3}$

Tuff adsorption isotherms were measured considering a reference regeneration temperature of 220 °C and three different equilibrium temperatures: 25 °C, 35 °C, and 50 °C. Results are shown in Figure 10. As expected, a consistent trend can be observed from lower (more efficient adsorption behavior) to higher (less efficient adsorption behavior) equilibrium temperatures.

For comparative purposes, adsorption isotherms of tuff and commercial 13X zeolites at 35 °C were also measured using regeneration temperatures of 220 °C and 350 °C (Figure 11). In this case, higher regeneration temperatures translate into an enhanced adsorption capacity. It can also be observed that tuff adsorption properties are lower than 13X, however close enough to make tuff an interesting alternative to synthetic zeolites. It is found, by chance, that 350 °C-regenerated tuff has similar properties of 220 °C-regenerated 13X.

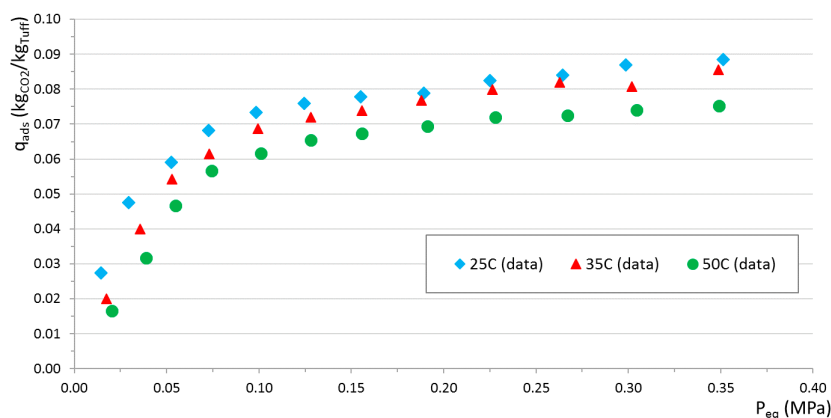


Figure 10. Adsorption isotherms for tuff (220 °C regeneration).

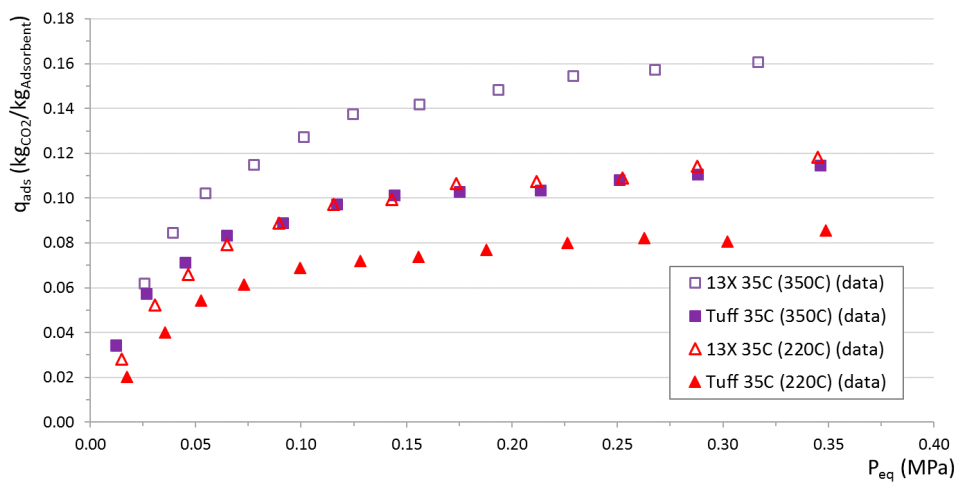


Figure 11. Adsorption isotherms for tuff and 13X at 35 °C (220 °C vs. 350 °C regeneration).

An estimate of tuff and 13X adsorption properties was finally produced fitting three common analytic parameterizations to observed data: Langmuir (Equation (9)), Langmuir-Freundlich (Equation (10)), and Toth (Equation (11)) models:

Langmuir isotherm [28]:

$$q = \frac{q_m \times B \times P}{1 + B \times P} \tag{9}$$

Langmuir-Freundlich isotherm [28]:

$$q = \frac{q_m \times (B \times P)^n}{1 + (B \times P)^n} \tag{10}$$

Toth isotherm [39]:

$$q = \frac{q_m \times B \times P}{[1 + (B \times P)^n]^{\frac{1}{n}}} \tag{11}$$

Fit results for tuff at 35 °C (220 °C regeneration) are shown in Figure 12. Best-fit values and probabilities for the three models are given in Tables 5–7.

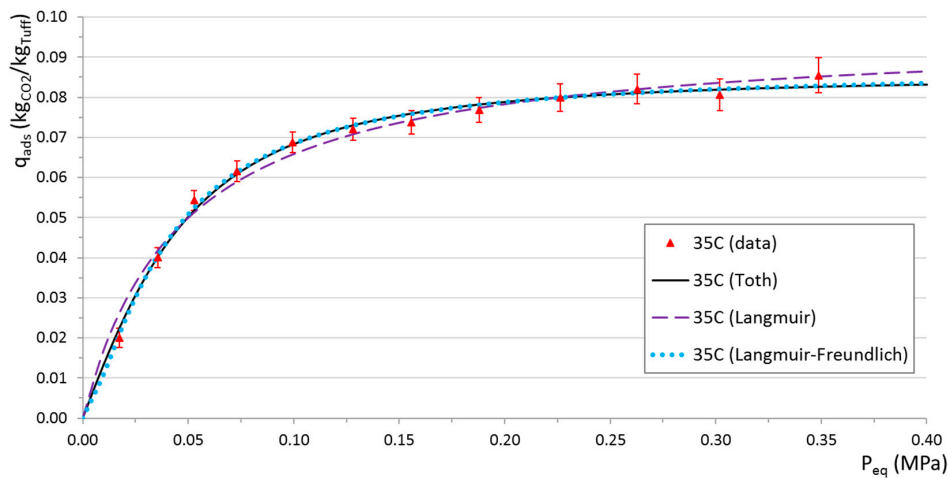


Figure 12. Fit of the three models to the tuff 35 °C isotherm (220 °C regeneration).

Table 5. Best-fit parameters and fit probabilities.

Toth Model						
Adsorbent	Eq. Temp. (C)	Reg. Temp. (C)	q_m (kgCO ₂ /kgAdsorbent)	B (MPa ⁻¹)	n (-)	Prob.
Tuff	25	220	0.0926 ± 0.0029	29.6 ± 3.5	1.10 ± 0.13	97.7%
Tuff	35	220	0.0854 ± 0.0022	16.2 ± 1.3	1.66 ± 0.23	93.3%
Tuff	50	220	0.0741 ± 0.0015	12.5 ± 0.7	2.49 ± 0.41	85.1%
Tuff	35	350	0.125 ± 0.004	35 ± 4	0.91 ± 0.09	98.1%
13X	35	220	0.124 ± 0.003	18.4 ± 1.3	1.27 ± 0.13	97.0%
13X	35	350	0.174 ± 0.004	18.3 ± 0.8	1.24 ± 0.08	95.0%

Table 6. Best-fit parameters and fit probabilities.

Langmuir						
Adsorbent	Eq. Temp. (C)	Reg. Temp. (C)	q_m (kgCO ₂ /kgAdsorbent)	B (MPa ⁻¹)	n (-)	Prob.
Tuff	25	220	0.0948 ± 0.0012	32.1 ± 1.8		97.8%
Tuff	35	220	0.097 ± 0.002	21 ± 2		30.0%
Tuff	50	220	0.090 ± 0.004	18 ± 3		0.5%
Tuff	35	350	0.1220 ± 0.0012	32.2 ± 1.4		98.8%
13X	35	220	0.133 ± 0.002	21.3 ± 1.2		77.2%
13X	35	350	0.187 ± 0.002	20.6 ± 0.9		62.3%

Table 7. Best-fit parameters and fit probabilities.

Langmuir-Freundlich						
Adsorbent	Eq. Temp. (C)	Reg. Temp. (C)	q_m (kgCO ₂ /kgAdsorbent)	B (MPa ⁻¹)	n (-)	Prob.
Tuff	25	220	0.0925 ± 0.0023	33.4 ± 2.1	1.08 ± 0.08	98.3%
Tuff	35	220	0.0866 ± 0.0016	25.6 ± 1.1	1.41 ± 0.09	98.9%
Tuff	50	220	0.0759 ± 0.0011	23.0 ± 0.7	1.75 ± 0.11	97.1%
Tuff	35	350	0.124 ± 0.003	31 ± 2	0.95 ± 0.06	98.0%
13X	35	220	0.125 ± 0.003	23.8 ± 1.2	1.17 ± 0.07	98.5%
13X	35	350	0.176 ± 0.003	23.1 ± 0.8	1.14 ± 0.04	97.7%

4. Discussion

The experimental campaign to characterize the adsorption properties of tuff clearly shows its suitability for CO₂ removal applications thanks to its interesting overall performance. It is found that, as is common for natural materials, and especially for byproducts, tuff is characterized by a broad range of particle sizes, resulting in an appreciable variability of porosity, skeletal and particle density, and pore diameter.

The fragility of this material is also responsible of a rapid wear of particles if not treated with the required care (i.e., minimizing friction during manipulation of the samples). No reduction of the particle average dimension (i.e., fractures) is observed, however, unlike 13X synthetic zeolites, dust is easily produced and it degrades the adsorption capacity if not properly removed during regeneration, which can be easily performed either with air or water. The mass loss during handling (loading, unloading, and treatment) is found to be less than 1% in weight after each cycle.

Thermal regeneration is found to play a major role in both tuff and 13X performance. A similar increase in the adsorption capacity of the two materials is found when the regeneration temperature is increased. Switching from 220 °C to 350 °C, the maximum adsorbable amount at 35 °C increases from approximately 0.085 to 0.125 kgCO₂/kgAdsorbent for tuff (+47%) and from approximately 0.125 to 0.175 kgCO₂/kgAdsorbent for 13X (+40%). Tuff clearly performs worse than 13X, however, it is close enough to represent a viable alternative, considering its negligible environmental impact and costs.

In this work just two regeneration temperatures were considered. It would be certainly interesting to find out the relation between the regeneration temperature and adsorption capacity, including an estimation of the excess thermal energy required for tuff regeneration to reach the same adsorption performance of 13X.

Saturation curves represent a key step of this analysis. Requiring CO₂ contamination in the outlet gas not exceeding 3%, it is found that approximately 0.03 kg_{CO₂}/kg_{Tuff} can be flown into the adsorber before the limit is crossed, in the most conservative case. Since before the breakthrough point the adsorption process is very efficient, this same value is also a good estimate of the maximum amount of CO₂ that tuff can adsorb before the outlet gas becomes CO₂-contaminated. The maximum adsorption capacity (i.e., full saturation) obtained from adsorption isotherms for a CO₂ partial pressure of approximately 0.05 MPa is between 0.045 kg_{CO₂}/kg_{Tuff} (50 °C) and 0.06 kg_{CO₂}/kg_{Tuff} (25 °C). As expected, this value is higher than that found with the saturation curves experiments. The adsorptive material, in fact, has to be replaced when the adsorption rate deteriorates: tuff particles are partly saturated and they are not able to contain the outlet CO₂ below 3%. This occurs after approximately 0.03 kg_{CO₂}/kg_{Tuff} are adsorbed, well before full saturation is reached.

It is found that tuff heterogeneity, once again, contributes to a certain spread of the adsorption effect in the transient regime. Nevertheless, a precise enough estimation of the breakthrough point is possible to produce also with a simple experimental apparatus as the one set up for this study. A very regular behavior of measured quantities is observed even with single-point measurements. The property characterization would benefit greatly from a more intensive campaign and from the analysis of more samples in order to produce a quantitative estimate of the heterogeneity effect on parameter estimation.

A dedicated section was included to show the results of a preliminary attempt to model the adsorption capacity of adsorbent particles in transient regime. An original phenomenological function is proposed to parameterize the adsorption rate as a function of the saturation level. It is clear how the proposed function describes, with good approximation, the behavior of the material around the breakthrough point and in terms of total adsorption capacity. It still lacks precision in the flattening region near the saturation. Future works will be dedicated to quantify the acceptance level of the hypothesis with an appropriate statistical analysis. Preliminary results, however, show that the proposed CFD model for selective gas adsorption can be reliably used to predict the system behavior at the breakthrough point over different boundary conditions.

Adsorption isotherms for tuff and 13X were produced using a second custom experimental apparatus. As for the saturation curves, because of the non-automated nature of the procedure, it was impossible to perform multiple measurements of single points, resulting in large uncertainties in best-fit parameter estimates. From the results using three different models, it is found that more complex three-parameter models (i.e., Toth and Langmuir-Freundlich) fit data with a remarkable quality (on average higher than 95% considering a chi-squared probability), while the simpler two-parameter model (Langmuir) sometimes fails in reproducing the observed data. The failure is more evident for those cases for which the exponential index n , computed with the other two models, is far from unity.

Preliminary results show a high heterogeneity of tuff physical properties. The characterization of the CO₂ adsorption performance clearly reflects the material variability. Design and sizing of an adsorption column for industrial applications will have to take into account this behavior. In a future development of this work, it would be interesting to increase the amount of collected data and to analyze a larger number of samples to quantitatively estimate the variability effect.

5. Conclusions

Tuff, a natural alternative to synthetic zeolites, was characterized with an intensive experimental campaign to prove its performance as a CO₂ adsorbent for biogas upgrading applications, carbon capture and sequestration, or other processes requiring a selective removal of carbon dioxide from a gaseous mixture.

The results of this work clearly shows that tuff can be effectively used for CO₂ adsorption. In order to measure tuff adsorption properties, several experimental activities were performed. Mercury porosimetry was used to determine the tuff physical properties according to common adsorbent classification parameters. Two different experimental apparatuses were used to perform an experimental characterization of tuff performance, both in transient and steady conditions.

Mercury intrusion porosimetry shows a particle porosity between 20.1% and 36.3%, a variable particle density between 977 and 1215 kg/m³, and an average pore diameter between 1.42 and 4.64 μm.

A saturation analysis in the transient regime was performed to relate the maximum amount of adsorbed CO₂ to a given maximum concentration of CO₂ in the purified (outlet) gas. Saturation curves were measured using a custom apparatus. A total of six tuff samples were analyzed, the inlet CO₂ concentration being approximately 50%. At atmospheric pressure and ambient temperatures, the breakthrough point (outlet CO₂ concentration of 3%) ranges from 0.029–0.036 kgCO₂/kg_{Tuff}. The adsorption process was also simulated using a CFD approach and proposing a phenomenological parameterization of the particle adsorption rate as a function of the saturation level. The simplified model was validated against observations.

An adsorption equilibrium analysis was performed to study the relationship between the maximum amount of adsorbed CO₂ and the main thermodynamic properties involved in the adsorption process. A second custom apparatus was set up allowing a precise measure up to approximately 0.4 MPa. The maximum amount of CO₂ adsorbed is highly influenced by the sample pretreatment (temperature during thermal regeneration) and operative conditions (equilibrium pressure and temperature) of the adsorption process. In this study, experimental isotherms as a function of the equilibrium pressure were measured for tuff at 25 °C, 35 °C, and 50 °C and two regeneration temperatures (220 °C and 350 °C). Three analytic models were fitted to observed data. Fit probabilities, on average higher than 95%, are found for three-parameter models, while the two-parameter model fails in some cases. It is found that tuff regenerated at 350 °C has the same adsorption capacity of 13X regenerated at 220 °C (0.125 kgCO₂/kg_{Adsorbent}), while it is approximately 70% that of 13X using the same regeneration temperature.

Future analyses should investigate a larger parameter space, in order to reproduce typical working conditions for PSA applications. In this context, CFD simulations of a fixed-bed adsorption for CO₂ removal, first proposed in this work, could represent a useful tool to test the performance of different design approaches and define the best configuration for industrial prototypes.

Acknowledgments: This work was supported by the Italian Ministry of the Environment and Protection of Land and Sea.

Author Contributions: Emanuele Bonamente and Andrea Aquino designed and realized custom equipment, performed laboratory tests, data analysis, and modeling. Andrea Nicolini and Franco Cotana supervised the research activity.

Conflicts of Interest: The authors declare no conflict of interest.

References

1. Allen, M.R.; Barros, V.R.; Broome, J.; Cramer, W.; Christ, R.; Church, J.A.; Clarke, L.; Dahe, Q.; Dasgupta, P.; Dubash, N.K.; et al. IPCC Fifth Assessment Synthesis Report—Climate Change 2014 Synthesis Report. Available online: <http://www.citeulike.org/group/15400/article/13416115> (accessed on 24 November 2016).
2. Bonamente, E.; Cotana, F. Carbon and Energy Footprint of Prefabricated Industrial Buildings: A systematic Life Cycle Assessment Analysis. *Energies* **2015**, *8*, 12685–12701. [[CrossRef](#)]
3. Rossi, F.; Bonamente, E.; Nicolini, A.; Anderini, E.; Cotana, F. A Carbon Footprint and energy consumption assessment methodology for UHI-affected lighting systems in built areas. *Energy Build.* **2015**, *114*, 96–103. [[CrossRef](#)]

4. Bonamente, E.; Rossi, F.; Coccia, V.; Pisello, A.L.; Nicolini, A.; Castellani, B.; Cotana, F.; Filipponi, M.; Morini, E.; Santamouris, M. An energy-balanced analytic model for urban heat canyons: Comparison with experimental data. *Adv. Build. Energy Res.* **2013**, *7*, 222–234. [[CrossRef](#)]
5. Bonamente, E.; Pelliccia, L.; Merico, M.C.; Rinaldi, S.; Petrozzi, A. The Multifunctional Environmental Energy Tower: Carbon Footprint and Land Use Analysis of an Integrated Renewable Energy Plant. *Sustainability* **2015**, *7*, 13564–13584. [[CrossRef](#)]
6. Yang, H.; Xu, Z.; Fan, M.; Gupta, R.; Slimane, R.B.; Bland, A.E.; Ian, W. Progress in carbon dioxide separation and capture: A review. *J. Environ. Sci.* **2008**, *20*, 14–27. [[CrossRef](#)]
7. Castellani, B.; Rossi, F.; Filipponi, M.; Nicolini, A. Hydrate-based removal of carbon dioxide and hydrogen sulphide from biogas mixtures: Experimental investigation and energy evaluations. *Biomass Bioenergy* **2014**, *70*, 330–338. [[CrossRef](#)]
8. McEwen, J.; Hayman, J.D.; Yazaydin, A.O. A comparative study of CO₂, CH₄ and N₂ adsorption in ZIF-8, Zeolite-13X and BPL activated carbon. *Chem. Phys.* **2013**, *412*, 72–76. [[CrossRef](#)]
9. Riboldi, L.; Bolland, O.; Ngoy, J.M.; Wagner, N. Full-plant Analysis of a PSA CO₂ Capture Unit Integrated In Coal-fired Power Plants: Post-and Pre-combustion Scenarios. *Energy Procedia* **2014**, *63*, 2289–2304. [[CrossRef](#)]
10. Sircar, S. Pressure Swing Adsorption. *Ind. Eng. Chem. Res.* **2002**, *41*, 1389–1392. [[CrossRef](#)]
11. Chen, S.J.; Fu, Y.; Huang, Y.X.; Tao, Z.C.; Zhu, M. Experimental investigation of CO₂ separation by adsorption methods in natural gas purification. *Appl. Energy* **2016**, *179*, 329–337. [[CrossRef](#)]
12. Ryckebosch, E.; Drouillon, M.; Vervaeren, H. Techniques for transformation of biogas to biomethane. *Biomass Bioenergy* **2011**, *35*, 1633–1645. [[CrossRef](#)]
13. Cotana, F.; Petrozzi, A.; Cavalaglio, G.; Coccia, V.; Pisello, A.L.; Bonamente, E. A Batch Digester Plant for Biogas Production and Energy Enhancement of Organic Residues from Collective Activities. *Energy Procedia* **2014**, *61*, 2841–2844. [[CrossRef](#)]
14. Jiajie, L.; Michael, H. Carbon dioxide adsorption isotherm study on mine waste for integrated CO₂ capture and sequestration processes. *Powder Technol.* **2007**, *291*, 408–413.
15. Weilong, W.; Jiang, L.; Xiaolan, W.; Jing, D.; Haijun, F.; Jinyue, Y.; Jianping, Y. Carbon dioxide adsorption thermodynamics and mechanisms on MCM-41 supported polyethylenimine prepared by wet impregnation method. *Appl. Energy* **2015**, *142*, 221–228.
16. Hao, Y.; Maochu, G.; Yaoqiang, C. Preparation of activated carbons and their adsorption properties for greenhouse gases: CH₄ and CO₂. *J. Natl. Gas Chem.* **2011**, *20*, 460–464.
17. Rad, M.D.; Shohreh, F.; Mojtaba, S.M. Development of T type zeolite for separation of CO₂ from CH₄ in adsorption processes. *Chem. Eng. Res. Des.* **2012**, *90*, 1687–1695. [[CrossRef](#)]
18. Hua, D.; Honghong, Y.; Xiaolong, T.; Qiongfeng, Y.; Ping, N.; Liping, Y. Adsorption equilibrium for sulfur dioxide, nitric oxide, carbon dioxide, nitrogen on 13X and 5A zeolites. *Chem. Eng. J.* **2012**, *188*, 77–85.
19. Youn-Sang, B.; Brad, G.H.; Omar, K.F.; Joseph, T.H.; Randall, Q.S. Enhancement of CO₂/CH₄ selectivity in metal-organic frameworks containing lithium cations. *Microporous Mesoporous Mater.* **2011**, *141*, 231–235.
20. Pinto, M.L.; Pires, J.; Roacha, J. Porous Materials Prepared from Clays for the Upgrade of Landfill Gas. *J. Phys. Chem. C* **2008**, *112*, 14394–14402. [[CrossRef](#)]
21. De Gennaro, M.; Cappelletti, P.; Langella, A.; Perrotta, A.; Scarpati, C. Genesis of zeolites in the Neapolitan Yellow Tuff: Geological, volcanological and mineralogical evidence. *Contrib. Mineral. Petrol.* **2000**, *139*, 17–35. [[CrossRef](#)]
22. Colella, C.; de Gennaro, M.; Aiello, R. Use of Zeolitic Tuff in the Building Industry. *Rev. Mineral. Geochem.* **2001**, *45*, 551–587. [[CrossRef](#)]
23. Giesche, H. Mercury Porosimetry: A General (Practical) Overview. *Part. Part. Syst. Charact.* **2006**, *23*, 1–11. [[CrossRef](#)]
24. Purewal, J. Hydrogen Adsorption by Alkali Metal Graphite Intercalation Compounds. Available online: <http://thesis.library.caltech.edu/5574/> (accessed on 27 September 2016).
25. Robert, H.P. *Perry's Chemical Engineers' Handbook*, 7th ed.; McGraw-Hill: New York, NY, USA, 2007.
26. Paolini, V.; Petracchini, F.; Guerriero, E.; Bencini, A.; Serena, D. Biogas clearing and upgrading with natural zeolites from tuffs. *Environ. Technol.* **2016**, *37*, 1418–1427. [[CrossRef](#)] [[PubMed](#)]
27. Alonso-Vicario, A.; Jose, R.O.; Gil-Rio, S.; Gomez-Jiménez-Aberasturi, O.; Ramirez-Lopez, C.A.; Torrecilla-Soria, J.; Dominguez, A. Purification and upgrading of biogas by pressure swing adsorption on synthetic and natural zeolites. *Microporous Mesoporous Mater.* **2010**, *134*, 100–107. [[CrossRef](#)]

28. Yang, R.T. *Adsorbents: Fundamentals and Applications*, 1st ed.; John Wiley & Sons: Hoboken, NJ, USA, 2003; pp. 8–22.
29. Ruthven, D.M. *Principles of Adsorption and Adsorption Processes*; John Wiley & Sons: Hoboken, NJ, USA, 1984; pp. 29–61.
30. Wang, Y.; De Carlo, F.; Mancini, D.C.; McNulty, I.; Tieman, B.; Bresnahan, J.; Foster, I.; Insley, J.; Lane, P.; Von Laszewski, G.; et al. A high-throughput X-ray microtomography system at the advanced photon source. *Rev. Sci. Instrum.* **2001**, *72*, 2062–2068. [[CrossRef](#)]
31. Koster, A.J.; Ziese, U.; Verkleij, A.J.; Janssen, A.H.; De Jong, K.P. Three-dimensional transmission electron microscopy: A novel imaging and characterization technique electron microscopy: A novel imaging and characterization technique with nanometer scale resolution for materials science. *J. Phys. Chem.* **2000**, *104*, 9368–9370. [[CrossRef](#)]
32. Hollewand, M.P.; Gladden, L.F. Heterogeneities in structure and diffusion within porous catalyst support pellets observed by NMR imaging. *J. Catal.* **1993**, *144*, 254–272. [[CrossRef](#)]
33. Rigby, S.P.; Daut, S. A statistical model for the heterogeneous structure of porous catalyst pellets. *Adv. Colloid Interface Sci.* **2002**, *98*, 87–119. [[CrossRef](#)]
34. Lestinsky, P.; Marek, V.; Peter, N.; Petr, S. The removal of CO₂ from biogas using a laboratory PSA unit: Design using breakthrough curves. *Clean Technol. Environ. Policy* **2015**, *17*, 1281–1289. [[CrossRef](#)]
35. Technical Report UNI/TR 11537:2016 Biomethane Injection in the Natural Gas Network. Available online: <http://infostore.saiglobal.com/EMEA/Details.aspx?ProductID=1885139> (accessed on 24 November 2016).
36. *ANSYS Fluent Flow User's Guide, Release 16.2*; Ansys, Inc.: Canonsburg, PA, USA, 2015.
37. *ANSYS Fluent Flow Theory Guide, Release 16.0*; Ansys, Inc.: Canonsburg, PA, USA, 2015.
38. Mohammad, S.S.; Wan, M.A.W.D.; Ahmad, S. A review of mathematical modeling of fixed-bed columns for carbon dioxide adsorption. *Chem. Eng. Res. Des.* **2014**, *92*, 961–988.
39. Cavenati, S.; Carlos, A.G.; Rodrigues, A.E. Adsorption Equilibrium of Methane, Carbon Dioxide, and Nitrogen on Zeolite 13X at High Pressures. *J. Chem. Eng.* **2004**, *49*, 1095–1101. [[CrossRef](#)]



© 2016 by the authors; licensee MDPI, Basel, Switzerland. This article is an open access article distributed under the terms and conditions of the Creative Commons Attribution (CC-BY) license (<http://creativecommons.org/licenses/by/4.0/>).